A Numerical Study of the Fluctuating Flowfield of a Uniformly Loaded Propeller

GARY R. HOUGH*
Therm Advanced Research Inc., Ithaca, N. Y.

A simple method has been developed for calculating the flowfield of a finite-bladed propeller in the forward flight regime. This method is based upon classical propeller vortex theory and the Fourier analysis of the resulting induced velocities. A numerical study of the harmonic content of the flowfield has been carried out for a uniformly loaded propeller for representative blade numbers and operating advance ratios. The results indicate that the fluctuating part of the velocity components is appreciable as compared to the steady, or time-independent, part for low blade numbers and/or high advance ratios. The total inflow at the propeller blades has also been calculated and correlated with the known analytical results for the steady inflow at the propeller plane.

Nomenclature

C_T = propeller thrust coefficient, $T/\frac{1}{2}\rho U^2\pi R^2$
$\mathbf{c}_m$ = Fourier harmonic coefficient of $\mathbf{q}$
J = advance ratio, $U/\Omega R$
m = harmonic number
N = number of propeller blades
$Q_{mN-1/2}(\omega)$ = Legendre function of the second kind and half-integer degree of argument ω
$\mathbf{q}$ = vector induced velocity
R = propeller radius
U = forward flight velocity
u, v, w = axial, radial, and tangential components, respectively, of induced velocity
x, r, θ = cylindrical propeller-fixed coordinate system
Γ = propeller blade circulation
Ω = propeller angular velocity
$\mathcal{R}, \mathcal{J}$ = defined in Eqs. (5, 13, and 18)
$\bar{(\ )}$ = steady part of induced velocity

Subscripts

b, t = contribution from bound and trailing vortices, respectively
m = harmonic number
p = value at propeller blade
0 = value at propeller plane

Superscripts

u, v, w = identifies axial, radial, and tangential velocity components, respectively

Introduction

IN recent years the rapid development of new V/STOL aircraft has been accompanied by renewed interest in the theory, design, and performance of propellers. In particular, detailed knowledge of the over-all propeller-induced flowfield is important for calculating the acoustic field, the loading on wings and other components located in the slipstream, and also for the design of propeller blades for optimum performance throughout the various flight regimes.

Recently, a new method for calculating the flowfield of a finite-bladed propeller in the forward flight regime has been developed.[1] It was based upon classical vortex theory of the propeller and the Fourier analysis of the corresponding induced velocity field. From this theory, results for the steady, or time-independent, part of the velocity components have been presented.[1,2] This steady part corresponds to the zeroth harmonic portion of the flowfield and was shown to be equivalent to the conventional actuator disk representation of the propeller, provided that the disk loading and advance ratio are the same.

In the present paper, the results of a numerical study of the harmonic content of the induced flowfield are presented. The calculations are carried out for a propeller having a uniform disk loading, or equivalently, a constant distribution of circulation along the blades. In outline, the basic formulation of the problem and the key steps in the Fourier analysis of the flowfield are presented first. Then, the calculation of the harmonic content and the behavior of the axial, radial, and tangential velocities is considered in detail. Finally, the total induced velocities at the propeller blades are calculated. They are compared with the known analytical results for the steady inflow at the propeller plane, and a simple empirical correlation is found between the two.

Basic Formulation

We consider a lightly-loaded propeller operating at zero incidence in a uniform, inviscid, incompressible stream of speed U. The propeller is taken to have N identical equally spaced blades of radius R which are rotating about their axis at a constant angular velocity Ω. A cylindrical, propeller-blade fixed coordinate system x, r, θ is chosen such that the propeller disk is normal to the x axis and is located at $x = 0$ (see Fig. 1). The propeller blades are located at $\theta_p = 2\pi(l - 1)/N$ where l is the ordinal number of the blade.

If we assume that both the blade thickness-to-chord and chord-to-radius ratios are small, the propeller can be well represented by the classical model of a bound radial vortex line of strength $\Gamma(\xi)$ for each blade accompanied by a helical sheet of vortices of strength $-d\Gamma/d\xi$ trailing from each line, where ξ is the radial distance to any element of the vortex line. Consistent with our assumptions, the helical path of the trailing vortex system is determined solely by the incoming freestream with translation U and rotation Ω. For simplicity in the analysis, the effects of the propeller hub are disregarded, although a finite hub could have been taken into account quite straightforwardly.

Now in the coordinate system chosen, the flow is periodic in θ (or equivalently in time since we can set $\theta = \Omega t$). That is, the velocity is composed of a steady component plus a

Received April 7, 1966; revision received June 29, 1966. This research was supported by the U. S. Army Research Office-Durham under Contract DA-31-124-ARO-D-374. The author wishes to thank M. D. Greenberg, J. C. Erickson Jr., and D. E. Ordway for their valuable suggestions and assistance during various portions of this work. The author also acknowledges the contribution of A. L. Kaskel in programing the equations for the digital computer.

* Staff Scientist. Member AIAA.

superimposed fluctuating component of period $2\pi/N\Omega$. Accordingly, we can express the total vector-induced velocity $\mathbf{q}$ at any field point in the complex Fourier series

$$\mathbf{q} = U \sum_{m=-\infty}^{\infty} \mathbf{c}_m(x, r)e^{imN\theta} \tag{1}$$

where $i = (-1)^{1/2}$ and the Fourier harmonic coefficients $\mathbf{c}_m$ are found from orthogonality as

$$\mathbf{c}_m = \frac{1}{2\pi U}\int_{-\pi}^{\pi} \mathbf{q}\, e^{-imN\theta}\, d\theta \tag{2}$$

Since $\mathbf{q}$ is a real quantity, $\mathbf{c}_m$ and $\mathbf{c}_{-m}$ must be complex conjugates for $m \neq 0$, and $\mathbf{c}_0$ is real.

We now separate $\mathbf{q}$ into its axial, radial, and tangential components u, v, and w, respectively, or

$$\mathbf{q} = u\mathbf{i}_x + v\mathbf{i}_r + w\mathbf{i}_\theta \tag{3}$$

and correspondingly

$$\mathbf{c}_m = c_m{}^u\mathbf{i}_x + c_m{}^v\mathbf{i}_r + c_m{}^w\mathbf{i}_\theta \tag{4}$$

where $\mathbf{i}_x$, $\mathbf{i}_r$ and $\mathbf{i}_\theta$ are the unit vectors in the x, r, and θ directions at the field point. To calculate u, v, and w, it is most convenient to consider the contributions from the bound and trailing vortices separately. Biot-Savart type calculations are performed to yield these contributions. The corresponding Fourier harmonic coefficients have been determined in integral form[1] in terms of Legendre functions of the second kind and half-integer degree since these functions have proven to be particularly useful in studies of the propeller velocity field. Expressions for the harmonic coefficients of the axial, radial, and tangential velocities taken from Ref. 1 are given in the Appendix.

In view of the complexity of these Fourier harmonic coefficients, analytical reduction to a simple closed form is not possible. However, if we assume a uniform disk loading, or equivalently, a constant blade circulation,† simplifications can be obtained in the expressions for the harmonic coefficients. It has been shown that the velocities outside of the propeller slipstream may be satisfactorily approximated with such an assumption. Moreover, the case of constant circulation provides a very convenient reference against which to compare calculations for other circulation distributions. For these reasons, we will hereafter consider the circulation Γ to be constant along the propeller blade. The trailing vortex system then reduces to a line vortex of strength $N\Gamma$ along the propeller axis and N helical vortices trailing from each of the blade tips.

As we have said, the steady, or time-independent, part of the induced-velocity field corresponding to $m = 0$ was studied extensively in Refs. 1 and 2. Calculations of these steady components at representative field points, as well as their limiting behavior, are contained there. We now turn to the study of the fluctuating part of the induced velocities in order to complete the description of the over-all flowfield. This requires the evaluation of the general Fourier harmonic coefficients $c_m{}^u$, $c_m{}^v$, and $c_m{}^w$, and we will consider each of the velocity components in turn.

Fluctuating Velocity Field

Axial Velocity

For the case of uniform loading, the expression for the Fourier harmonic coefficient can be simplified as outlined in the Appendix. We find that both the bound blade vortices and those trailing from the blade tips contribute to the nonsteady part of the induced axial velocity.‡ If we distinguish these contributions by the subscripts b and t, respectively, then we can show that

$$c_m{}^u = JC_T\{\mathcal{R}_t{}^u - i(\mathcal{I}_t{}^u + \mathcal{I}_b{}^u)\} \tag{5}$$

where J is the propeller advance ratio $J \equiv U/\Omega R$, C_T is the ideal propeller thrust coefficient $C_T = N\Gamma/\pi JUR$, and

$$\mathcal{R}_t{}^u \equiv \frac{1}{8\pi r^{3/2}}\int_0^\infty \{rQ_{mN+1/2}{}'(\omega_1) + rQ_{mN-3/2}{}'(\omega_1) - 2Q_{mN-1/2}{}'(\omega_1)\}\cos mN\tau\, d\tau \tag{6}$$

$$\mathcal{I}_t{}^u \equiv \frac{1}{8\pi r^{3/2}}\int_0^\infty \{rQ_{mN+1/2}{}'(\omega_1) + rQ_{mN-3/2}{}'(\omega_1) - 2Q_{mN-1/2}{}'(\omega_1)\}\sin mN\tau\, d\tau \tag{7}$$

$$\mathcal{I}_b{}^u \equiv \frac{mN}{4\pi r^{1/2}}\int_0^1 \xi^{-3/2}\, Q_{mN-1/2}(\omega_2)\, d\xi \tag{8}$$

$Q_{mN-1/2}$ is the Legendre function of the second kind and half-integer degree, and we have expressed all lengths in units of propeller radii. The prime $(\ )'$ denotes differentiation with respect to the indicated argument, and the arguments of the Legendre functions are given by

$$\begin{aligned}\omega_1 &\equiv 1 + [(x - J\tau)^2 + (r - 1)^2]/2r \\ \omega_2 &\equiv 1 + [x^2 + (r - \xi)^2]/2r\xi\end{aligned} \tag{9}$$

Before proceeding with the evaluation of $\mathcal{R}_t{}^u$, $\mathcal{I}_t{}^u$, and $\mathcal{I}_t{}^u$, we state briefly some of their properties. First, note that $\mathcal{I}_b{}^u$ is a function of mN and the coordinates x and r, whereas $\mathcal{R}_t{}^u$ and $\mathcal{I}_t{}^u$ both depend on J as well. The limiting spatial and harmonic behavior of these quantities is found from appropriate expansions[3] of the Legendre functions as

$$\left.\begin{aligned}\lim_{r\to\infty} \mathcal{R}_t{}^u, \mathcal{I}_t{}^u, \mathcal{I}_b{}^u &= 0 \\ \lim_{r\to 0} \mathcal{R}_t{}^u, \mathcal{I}_t{}^u, \mathcal{I}_b{}^u &= 0 \\ \lim_{x\to-\infty} \mathcal{R}_t{}^u, \mathcal{I}_t{}^u, \mathcal{I}_b{}^u &= 0 \\ \lim_{mN\to\infty} \mathcal{R}_t{}^u, \mathcal{I}_t{}^u, \mathcal{I}_b{}^u &= 0\end{aligned}\right\} \tag{10}$$

and, in addition, $\mathcal{I}_b{}^u$ is symmetric in x. We can also show that both $\mathcal{R}_t{}^u$ and $\mathcal{I}_t{}^u$ are periodic in x, with period $2\pi J/mN$, sufficiently far downstream of the propeller plane.

Equations (6–8) cannot be integrated analytically and so must be evaluated numerically. Fortunately, this can be done quite straightforwardly. To compute $\mathcal{R}_t{}^u$, $\mathcal{I}_t{}^u$, and

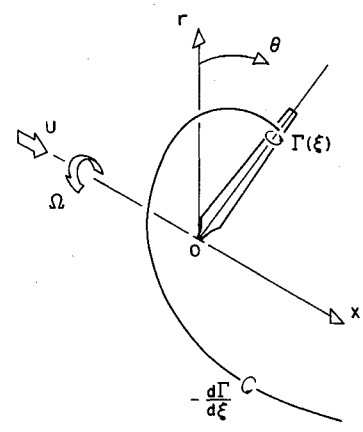

Fig. 1 Coordinate system and nomenclature.

† Note, however, that the condition of constant circulation implies that the angular velocity imparted to the air near the x axis is greater than the angular velocity of the propeller itself.

‡ The trailing vortices along the x axis give rise to a steady tangential induced velocity only.

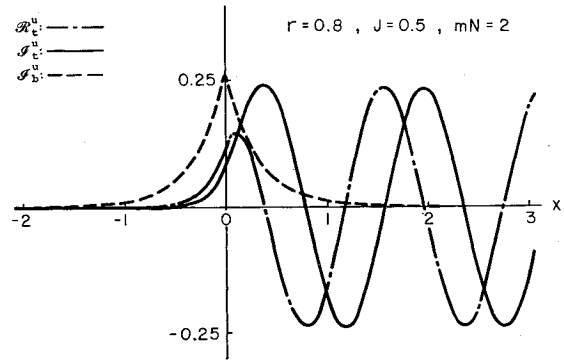

Fig. 2 Illustrative spatial variation of $\mathcal{R}_t^u$, $\mathcal{I}_t^u$, and $\mathcal{I}_b^u$.

$\mathcal{I}_b^u$, it is necessary to have a means of calculating the Legendre functions and their derivatives; this is done as follows. Both $Q_{-1/2}(\omega)$ and $Q_{1/2}(\omega)$ are simply expressed[4] in terms of the complete elliptic integrals $K[\{2/(\omega + 1)\}^{1/2}]$ and $E[\{2/(\omega + 1)\}^{1/2}]$, which in turn can be rationally approximated.[4] Knowing $Q_{-1/2}$ and $Q_{1/2}$ we can find $Q_{3/2}$ and subsequently $Q_{5/2}$, $Q_{7/2}$, . . . and their derivatives by recursion formulas.[5] Because of the errors that accumulate with successive applications of the recursion relationships at higher values of ω, it is necessary to supplement these relationships with a large argument expansion[3] for the $Q_{mN-1/2}$ and $Q_{mN-1/2}'$. In all cases considered, however, both of these functions were computed to an accuracy of at least $\pm 1 \times 10^{-4}$.

Equations (6–8) were evaluated on a CDC 1604 digital computer by a specially programed, multiple 10-point Gaussian technique with guaranteed accuracy. With mN and J specified, calculation of $\mathcal{R}_t^u$, $\mathcal{I}_t^u$, and $\mathcal{I}_b^u$ at a given field point generally takes less than one minute of running time. The calculations were carried out at a large number of representative field points for $J = \frac{1}{4}, \frac{1}{2}, 1$, and for $mN = 2, 3, 4, \ldots 12$ to cover a range of operating conditions and blade number/harmonic number combinations. In order to provide a check on the computer program, several cases were done by hand on a desk calculator.

In general, upstream of the propeller there is a rapid decay in $\mathcal{R}_t^u$, $\mathcal{I}_t^u$, and $\mathcal{I}_b^u$ with increasing distance from the propeller plane, and the coefficients become vanishingly small within approximately two radii. Downstream of the propeller, the calculations verify the predicted harmonic behavior of $\mathcal{R}_t^u$ and $\mathcal{I}_t^u$ with x; this appears to be fully established within an axial distance of about one propeller radius. Typical results for the axial variation of these coefficients are shown in Fig. 2. As mN increases, the coefficients get progressively smaller and essentially are zero by the time $mN = 12$ except within the very immediate vicinity of the propeller tip. The dependence of $\mathcal{R}_t^u$ and $\mathcal{I}_t^u$ on J is somewhat more complex but, in general, these coefficients decrease in magnitude as J increases.

With these techniques for the rapid calculation of c_m^u, the fluctuating part $(u - \bar{u})$ of the axial induced velocity is simply determined. We have

$$u = U \sum_{m=-\infty}^{\infty} c_m^u \, e^{imN\theta} \tag{11}$$

and using the fact that c_m^u and c_{-m}^u are complex conjugates, together with Eq. (5), yields

$$u - \bar{u} = 2UJC_T \left\{ \sum_{m=1}^{\infty} \mathcal{R}_t^u \cos mN\theta + \sum_{m=1}^{\infty} (\mathcal{I}_t^u + \mathcal{I}_b^u) \sin mN\theta \right\} \tag{12}$$

where $\bar{u}$ is the steady axial induced velocity corresponding to $m = 0$ and is given explicitly in Ref. 2.

Calculation of the azimuthal variation of u at several field points has been carried out for various combinations of blade number and operating advance ratio. From these calculations, we have found that the harmonic content is appreciable compared to the steady part for low blade numbers and/or high advance ratios. Figure 3 shows the θ variation of u with blade number at a representative field point; Fig. 4, the variation with advance ratio. We see, for example, that the peak-to-peak variation of u is over five times the mean value $\bar{u}$ for a two-bladed propeller at the point considered and that this ratio decreases rapidly with increasing N.

It is also of interest to compare these results for the variation of u with those obtained by including only the blade-frequency contribution, i.e., the $\cos N\theta$ and $\sin N\theta$ terms.§ This is done in Fig. 5, where the inclusion of all the blade harmonics results in a small increase in the peak-to-peak value of u although values of u at many θ locations differ by a large percentage. The over-all shape of the two curves is reasonably similar. For field points very near to the propeller tips, calculations of the induced velocity based on the blade-frequency contribution only will probably not yield satisfactory results.

Radial Velocity

Analogously to the axial velocity, the Fourier harmonic coefficient of the radial induced velocity can be reduced for the case of uniform loading to

$$c_m^v = JC_T\{\mathcal{R}_t^v - i(\mathcal{I}_t^v + \mathcal{I}_b^v)\} \tag{13}$$

where

$$\mathcal{R}_t^v \equiv \frac{-1}{8\pi r^{3/2}} \int_0^{\infty} \{(x - J\tau)[Q_{mN+1/2}'(\omega_1) + Q_{mN-3/2}'(\omega_1)] \cos mN\tau + J[Q_{mN-3/2}'(\omega_1) - Q_{mN+1/2}'(\omega_1)] \sin mN\tau\} d\tau \tag{14}$$

$$\mathcal{I}_t^v \equiv \frac{-1}{8\pi r^{3/2}} \int_0^{\infty} \{(x - J\tau)[Q_{mN+1/2}'(\omega_1) + Q_{mN-3/2}'(\omega_1)] \sin mN\tau - J[Q_{mN-3/2}'(\omega_1) - Q_{mN+1/2}'(\omega_1)] \cos mN\tau\} d\tau \tag{15}$$

and

$$\mathcal{I}_b^v = -(x/r)\mathcal{I}_b^u \tag{16}$$

The limiting behavior of $\mathcal{R}_t^v$, $\mathcal{I}_t^v$, and $\mathcal{I}_b^v$ is identical with their axial counterparts as given in Eqs. (10) and again $\mathcal{R}_t^v$ and $\mathcal{I}_t^v$ are harmonic in x sufficiently far downstream of the propeller. Now, however, $\mathcal{I}_b^v$ is antisymmetric in x.

The preceding integrals were evaluated in the same manner as were the axial components. Essentially the same general

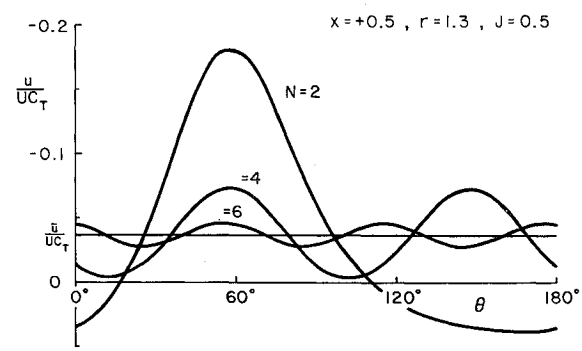

Fig. 3 Illustrative variation of axial induced velocity with blade number.

§ This approximate method for calculation of the induced velocity field has been employed previously by Breslin.[6]

over-all behavior is found as for the corresponding axial coefficients.

The fluctuating part $(v - \bar{v})$ of the induced radial velocity is found to be

$$v - \bar{v} = 2UJC_T \left\{ \sum_{m=1}^{\infty} \mathcal{R}_t{}^v \cos mN\theta + \sum_{m=1}^{\infty} (\mathcal{I}_t{}^v + \mathcal{I}_b{}^v) \sin mN\theta \right\} \quad (17)$$

where $\bar{v}$ is the steady radial induced velocity and is given explicitly in Ref. 2. The variation of v with θ has been calculated at a number of field points, and we find that the harmonic content is again appreciable compared to the steady value at low blade numbers and high advance ratios. Figure 6 compares the variation of the axial and radial velocities u and v just downstream of the propeller plane.

Tangential Velocity

By proceeding along the same lines as for the axial component, we can show that the Fourier harmonic coefficient of the tangential induced velocity is

$$c_m{}^w = JC_T\{(\mathcal{R}_t{}^w + \mathcal{R}_b{}^w) - i\mathcal{I}_t{}^w\} \quad (18)$$

where

$$\mathcal{R}_t{}^w \equiv \frac{1}{8\pi r^{3/2}} \int_0^{\infty} \{-(x - J\tau)[Q_{mN-3/2}'(\omega_1) - Q_{mN+1/2}'(\omega_1)] \sin mN\tau + J[Q_{mN-3/2}'(\omega_1) - 2rQ_{mN-1/2}'(\omega_1) + Q_{mN+1/2}'(\omega_1)] \cos mN\tau\} d\tau \quad (19)$$

$$\mathcal{R}_b{}^w \equiv \frac{x}{8\pi r^{3/2}} \int_0^1 \xi^{-3/2}\{Q_{mN+1/2}'(\omega_2) + Q_{mN-3/2}'(\omega_2)\} d\xi \quad (20)$$

$$\mathcal{I}_t{}^w \equiv \frac{1}{8\pi r^{3/2}} \int_0^{\infty} \{(x - J\tau)[Q_{mN-3/2}'(\omega_1) - Q_{mN+1/2}'(\omega_1)] \cos mN\tau + J[Q_{mN-3/2}'(\omega_1) - 2rQ_{mN-1/2}'(\omega_1) + Q_{mN+1/2}'(\omega_1)] \sin mN\tau\} d\tau \quad (21)$$

Again, the limiting behavior of these functions is equivalent to the axial velocity results, Eqs. (10). We find that $\mathcal{R}_b{}^w$ is antisymmetric in x and $\mathcal{R}_t{}^w$ and $\mathcal{I}_t{}^w$ are harmonic in x downstream of the propeller.

The fluctuating part of the tangential induced velocity $(w - \bar{w})$ can be written in the same form as its axial and radial counterparts and is

$$w - \bar{w} = 2UJC_T \left\{ \sum_{m=1}^{\infty} (\mathcal{R}_t{}^w + \mathcal{R}_b{}^w) \cos mN\theta + \sum_{m=1}^{\infty} \mathcal{I}_t{}^w \sin mN\theta \right\} \quad (22)$$

where $\bar{w}$ is the steady tangential induced velocity (see Ref. 2). Although the steady part $\bar{w}$ vanishes outside the propeller slipstream, the fluctuating component does not.

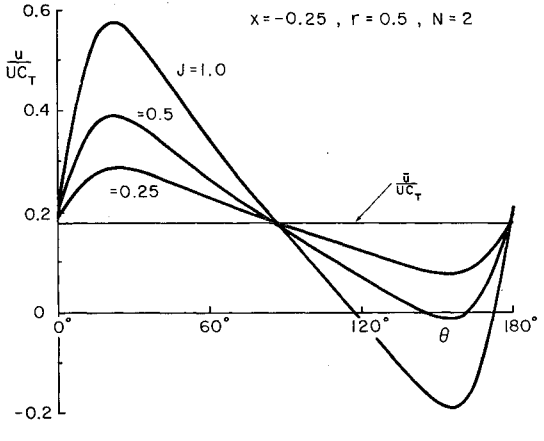

Fig. 4 Illustrative variation of axial induced velocity with advance ratio.

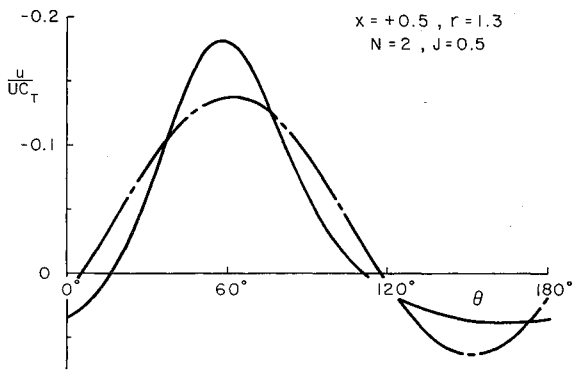

Fig. 5 Comparison of axial induced velocity determined from blade-frequency harmonic only (— - —) and from all harmonics (————).

Propeller Inflow

It is important for the propeller designer to have available a simple method for calculating accurately the induced inflow at the propeller blades so that performance characteristics may be determined.

We already know[2] that the steady axial and tangential inflow components at the propeller plane $\bar{u}_0$ and $\bar{w}_0$ are given by

$$\bar{u}_0 = UC_T/4 \quad (23)$$

and

$$\bar{w}_0 = -UJC_T/4r \quad (24)$$

Unfortunately, no simple formulas for u and w at the blades themselves can be derived and, consequently, they must be computed numerically as outlined in the previous section. Some simplifications can be made, however.

First, we consider the axial inflow at the propeller blades u_p and find from Eq. (12) and the fact that the blades are

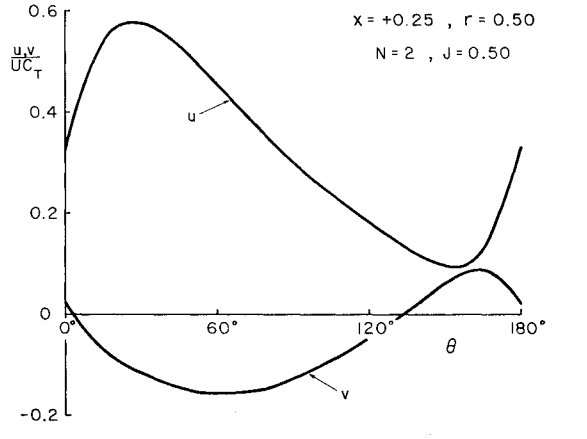

Fig. 6 Illustrative comparison of axial and radial induced velocities.

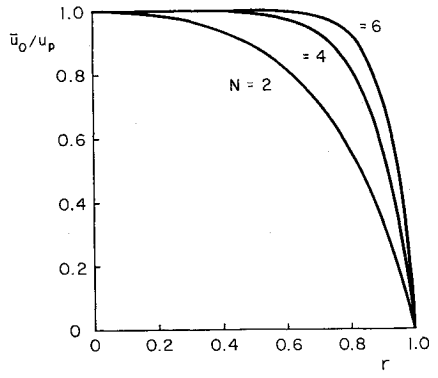

a) Variation with N, $J = 0.5$

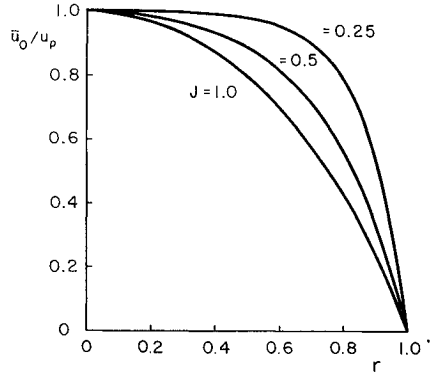

b) Variation with J, $N = 2$

Fig. 7 Ratio of steady axial velocity at propeller plane to axial velocity at propeller blade.

located at $\theta_p = 2\pi(l-1)N$ that

$$u_p - \bar{u}_0 = 2UJC_T \sum_{m=1}^{\infty} \mathcal{R}_t{}^u \tag{25}$$

where $\mathcal{R}_t{}^u$ is evaluated at $x = 0$. Substitution of Eq. (23) into Eq. (25) yields

$$\frac{\bar{u}_0}{u_p} = 1 \Big/ \left(1 + 8J \sum_{m=1}^{\infty} \mathcal{R}_t{}^u\right) \tag{26}$$

for the ratio of the steady axial velocity at the propeller plane to the axial velocity at the blades. This ratio has been calculated for several values of blade number N and advance ratio J, and some of the results are shown in Fig. 7. We see that as N increases and/or J decreases, the velocity at the blades tends toward the steady value. This is to be expected since, for these cases, the trailing vortex sheets become more "packed-in" and approach a continuum.

We have been able to approximate the computed results by the following empirical formulas:

$$\bar{u}_0/u_p = 1 - \exp\{-(4.1N - 0.5)(1 - r)\} \qquad J = \tfrac{1}{4} \tag{27}$$

$$\bar{u}_0/u_p = 1 - \exp\{-(2.3N - 0.3)(1 - r)\} \qquad J = \tfrac{1}{2} \tag{28}$$

Equation (27) is in error by at most 1%, Eq. (28) by at most 5% along the blades. These simple correlation formulas then, in conjunction with Eq. (23), provide an extremely simple method for determining the *total* axial blade inflow. It is hoped that future work will yield a single formula of the preceding form with the effect of J included explicitly in the exponential factor.

The determination of the tangential induced velocity at the propeller blades w_p follows analogously to the axial component, and we find that

$$\frac{\bar{w}_0}{w_p} = 1 \Big/ \left(1 - 8r \sum_{m=1}^{\infty} \mathcal{R}_t{}^w\right) \tag{29}$$

where $\bar{w}_0$ is given by Eq. (24) and $\mathcal{R}_t{}^w$ is calculated at $x = 0$.

Now, from Eqs. (23) and (24), we see that the resultant steady velocity at the propeller plane is perpendicular to the resultant freestream vector there, that is

$$\bar{u}_0/\bar{w}_0 = -r/J \tag{30}$$

This same result for the total inflow at the blades was established some time ago by Moriya.[7] Thus we conclude that the resultant of the fluctuating parts of u_p and w_p must likewise be perpendicular to the resultant freestream. Also, it follows that

$$\bar{u}_0/u_p = \bar{w}_0/w_p \tag{31}$$

and our numerical calculations of these ratios as given in Eqs. (26) and (29) verify this relationship. Moreover, our results reveal that

$$c_m{}^u(0, r) = -(r/J)c_m{}^w(0, r) \tag{32}$$

The ratio of the steady value at the propeller plane to the value at the propeller blades for the radial velocity component also can be calculated straightforwardly from our work, and some typical results are depicted in Fig. 8. From these calculations we find that the radial inflow at the blades is always less than the steady component especially for small blade numbers and high advance ratios. This contrasts with the axial and tangential inflow results in which the velocity at the blades is always greater than the steady part at the propeller plane.

Conclusions

From this numerical study of the fluctuating flowfield of a uniformly loaded propeller we conclude the following. First, the nonsteady part of the axial, radial, and tangential induced velocities may be calculated straightforwardly and rapidly on a digital computer for points everywhere in the flowfield except those in the very immediate vicinity of the propeller blade tips. For example, the running time on a CDC 1604 computer was on the order of one to two minutes per velocity component per field point.

Second, the harmonic content of these velocity components may be appreciable in comparison to the steady value particularly at low blade numbers and high advance ratios.

Finally, and probably most important for propeller design

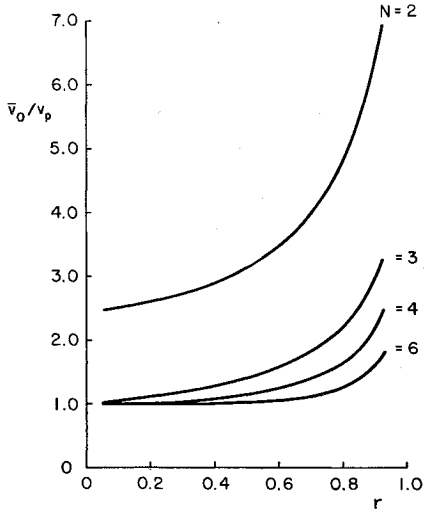

Fig. 8 Ratio of steady radial velocity at propeller plane to radial velocity at propeller blade, $J = 0.5$.

applications, the total inflow at the propeller blades can be expressed simply in terms of a correlation formula and the known analytical results for the steady inflow at the propeller plane.

Appendix

The contributions to the Fourier harmonic coefficients of the axial, radial, and tangential induced velocities $c_m{}^u$, $c_m{}^v$, and $c_m{}^w$ from the bound and trailing vortex systems are taken from Ref. 1 and listed below with x and r given in units of propeller radii.

For the contribution from the bound blade vortices we have:

$$c_{\Gamma m}{}^u = \frac{-iN}{8\pi^2 r^{1/2}} \int_0^1 \frac{\Gamma}{UR} \{Q_{mN+1/2}'(\omega_2) - Q_{mN-3/2}'(\omega_2)\} \xi^{-3/2} d\xi \tag{A1}$$

$$c_{\Gamma m}{}^v = \frac{iNx}{8\pi^2 r^{3/2}} \int_0^1 \frac{\Gamma}{UR} \{Q_{mN+1/2}'(\omega_2) - Q_{mN-3/2}'(\omega_2)\} \xi^{-3/2} d\xi \tag{A2}$$

$$c_{\Gamma m}{}^w = \frac{Nx}{8\pi^2 r^{3/2}} \int_0^1 \frac{\Gamma}{UR} \{Q_{mN+1/2}'(\omega_2) + Q_{mN-3/2}'(\omega_2)\} \xi^{-3/2} d\xi \tag{A3}$$

For the contribution from the trailing blade vortices we have:

$$c_{\Gamma' m}{}^u = \frac{-N}{8\pi^2 r^{3/2}} \int_0^1 \frac{\Gamma'}{U} \xi^{-1/2} \int_0^\infty \{rQ_{mN+1/2}'(\omega_3) + rQ_{mN-3/2}'(\omega_3) - 2\xi Q_{mN-1/2}'(\omega_3)\} e^{-imN\tau} d\tau d\xi \tag{A4}$$

$$c_{\Gamma' m}{}^v = \frac{N}{8\pi^2 r^{3/2}} \int_0^1 \frac{\Gamma'}{U} \xi^{-1/2} \int_0^\infty \{(x - J\tau - iJ) \times Q_{mN+1/2}'(\omega_3) + (x - J\tau + iJ) Q_{mN-3/2}'(\omega_3)\} e^{-imN\tau} d\tau d\xi \tag{A5}$$

$$c_{\Gamma' m}{}^w = \frac{-N}{8\pi^2 r^{3/2}} \int_0^1 \frac{\Gamma'}{U} \xi^{-1/2} \int_0^\infty \left\{(J + ix - iJ\tau) \times Q_{mN+1/2}'(\omega_3) + (J - ix + iJ\tau) Q_{mN-3/2}'(\omega_3) - \frac{2Jr}{\xi} Q_{mN-1/2}'(\omega_3)\right\} e^{-imN\tau} d\tau d\xi \tag{A6}$$

where ω_2 is given in Eq. (9) and

$$\omega_3 \equiv 1 + \frac{(x - J\tau)^2 + (r - \xi)^2}{2r\xi} \tag{A7}$$

For the case of constant blade circulation, these expressions can be simplified and combined to the forms given in Eqs. (5, 13, and 18). For the axial component $c_m{}^u$ we will illustrate how the functions $\mathcal{R}_t{}^u$, $\mathcal{I}_t{}^u$, and $\mathcal{I}_b{}^u$ are obtained. The other components follow in a similar fashion.

First, we note that if the tangential inflow at the propeller is neglected, the ideal propeller thrust coefficient C_T is given in terms of Γ by

$$C_T = N\Gamma/\pi JUR \tag{A8}$$

For the contribution of the bound vortices, the constant Γ can be taken outside the integral. Then, upon substitution of Eq. (A8) and the identity

$$Q_{mN+1/2}'(\omega) - Q_{mN-3/2}'(\omega) \equiv 2mNQ_{mN-1/2}(\omega) \tag{A9}$$

into Eq. (A1), we obtain the function $JC_T\mathcal{I}_b{}^u$. For the trailing vortex contribution we can write Eq. (A4) in the form

$$c_{\Gamma' m}{}^u = N \int_0^1 G_{mN}(x, r;\ J;\ \xi)\Gamma'(\xi)\, d\xi = -N\Gamma G_{mN}(x, r;\ J;\ 1) - N\Gamma G_{mN}(x, r;\ J;\ 0) \tag{A10}$$

and then show that $G_{mN}(x, r;\ J;\ 0) = 0$.¶ The functions $JC_T\,\mathcal{R}_t{}^u$ and $JC_T\mathcal{I}_t{}^u$ are found by substituting Eq. (A8) into Eq. (A10), separating the exponential factor of $G_{mN}(x, r;\ J;\ 1)$ into its real and imaginary parts, and simplifying the results.

References

[1] Hough, G. R. and Ordway, D. E., "The generalized actuator disk," *Developments in Theoretical and Applied Mechanics* (Pergamon Press, Oxford, England, 1965), Vol. 2, pp. 317–336.

[2] Hough, G. R. and Ordway, D. E., "The steady velocity field of a propeller with constant circulation distribution," J. Am. Helicopter Soc. **10**, 27–28 (April 1965).

[3] Sluyter, M. M., "A computational program and extended tabulation of Legendre functions of second kind and half order," THERM Inc., Ithaca, N. Y., TAR-TR 601 and Suppl. (October 1960).

[4] Abramowitz, M. and Stegun, I. A. (eds.), *Handbook of Mathematical Functions* (National Bureau of Standards, Washington, D. C., 1964), AMS 55, Chaps. 8 and 17, pp. 337, 591–592.

[5] Whittaker, E. T. and Watson, G. N., *A Course of Modern Analysis* (Cambridge University Press, Cambridge, 1963), Chap. XV, p. 318.

[6] Breslin, J. P., "Review and extension of theory for near-field propeller-induced vibratory effects," *Fourth Symposium on Naval Hydrodynamics* (U. S. Government Printing Office, Washington, D. C.), ACR-92, pp. 603–640.

[7] Moriya, T., "On the integration of Biot-Savart's law in propeller theory," J. Soc. Aeronaut. Sci. Japan **9**, 1015–1020 (1942).

¶ This must be true since the vortices trailing along the propeller centerline cannot contribute to the axial velocity component.